

pubs.acs.org/JACS Article

Real-Time Monitoring of the Structural Transition of *Bombyx mori* Liquid Silk under Pressure by Solid-State NMR

Yu Suzuki,* Shota Morie, Hideyasu Okamura, Tetsuo Asakura, and Akira Naito*



Cite This: J. Am. Chem. Soc. 2023, 145, 22925–22933



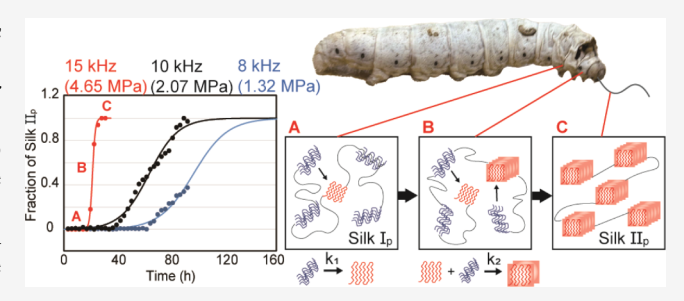
ACCESS I

III Metrics & More

Article Recommendations

s Supporting Information

ABSTRACT: Silk fibroin is stored in the silk glands of *Bombyx mori* silkworms as a condensed aqueous solution called liquid silk. It is converted into silk fibers at the silkworm's spinnerets under mechanical forces including shear stress and pressure. However, the detailed mechanism of the structural transition of liquid silk to silk fibers under pressure is not well understood. Magic angle spinning (MAS) in solid-state nuclear magnetic resonance (NMR) can exert pressure on liquid samples in a quantitative manner. In this study, solid-state NMR was used to quantitatively analyze the impact of pressure on the structural transition of liquid silk. A



combination of 13 C DD-MAS and CP-MAS NMR measurements enabled the conformation and dynamics of the crystalline region of the silk fibroin (both before (Silk I_p) and after (Silk II_p) the structural transition) to be detected in real time with atomic resolution. Spectral analyses proposed that the pressure-induced structural transition from Silk I_p to Silk II_p proceeds by a two-step autocatalytic reaction mechanism. The first reaction step is a nucleation step in which Silk I_p transforms to single lamellar Silk II_p , and the second is a growth step in which the single lamellar Silk II_p acts as a catalyst that reacts with Silk I_p molecules to further form Silk II_p molecules, resulting in stacked lamellar Silk II_p . Furthermore, the rate constant in the second step shows a significant pressure dependence, with an increase in pressure accelerating the formation of large stacked lamellar Silk II_p .

1. INTRODUCTION

Silkworms produce silk fibers from aqueous silk solutions at ambient temperatures. As these fibers exhibit high strength, toughness, and biodegradability, significant attention has been directed toward investigating the process of fiber formation in silkworms. The goal is to understand the mechanism by which these robust fibers are produced naturally and how such processes can be replicated on an industrial scale. 1–3

The silk of *Bombyx mori* (*B. mori*) silkworms is composed of two proteins: fibroin, which constitutes the fibers, and sericin, which coats and adheres to the fibers. The fibroin molecule consists of a 390 kDa heavy (H) chain, a 26 kDa light (L) chain, and a glycoprotein, P25. The H and L chains are connected by disulfide bonds, while P25 molecules associate with the disulfide-linked H and L chains via noncovalent interactions. The predominant amino acids in the H chain are glycine (Gly; 42.9%), alanine (Ala; 30.0%), serine (Ser; 12.2%), and tyrosine (Tyr; 4.8%). The H chain consists of two hydrophilic N- and C-terminal domains and a highly repetitive sequence that consists of 12 repeating Gly- and Ala-rich domains interspersed with conserved linker sequences in between.

The secondary structures of fibroin before and after the structural transition are termed Silk I and Silk II, respectively. Silk I has a repeated type II β -turn structure, as determined by atomic-level conformational analysis via solid-state NMR of model peptides, 7^{-11} and this result is supported by the solution

NMR structural analysis of intact liquid silk. ¹² In contrast, X-ray crystallography results indicate that Silk II has an antiparallel β -sheet structure. Interestingly, Marsh et al. ¹³ reported that the antiparallel β -sheets are stacked in a polar manner, while Takahashi et al. ¹⁴ reported that they are stacked in an antipolar manner. Subsequently, solid-state NMR studies with model peptides mimicking the fibroin crystal region have suggested that Silk II has a lamellar structure consisting of eight residue-length β -strands connected with turn structures in an antipolar manner. ^{15–17}

The structural transition in natural fiber spinning involves several steps. The structure and function of the silk gland of a silkworm are shown in Figure S1. ¹⁸ The silk gland consists of a narrow diverging posterior part (1), a wider S-shaped middle part (2), and a narrow anterior part (3). The spinneret also consists of three parts: a common tube (4), a silk press (5), and a spinning tube (6). Fibroin molecules are secreted into the posterior part as an aqueous solution known as liquid silk, stored in the middle part, and flowed to the anterior part. In

Received: April 27, 2023 Published: October 13, 2023





the silk gland, fibroin fiber formation is induced by a combination of pH changes, ionic environment, ^{19,20} and mechanical forces. ^{21,22} However, the mechanism of the fibroin fiber formation is not fully understood.

Many studies have been conducted to understand the structural transitions that occur during silk fiber formation by examining the influence of fibroin flow and the resulting shear stress.²³⁻³³ Several simulation analyses have shown that extrusion pressures greater than 30 MPa are required to generate the shear stress to fibrillate fibroin at natural spinning rates (0.02 m/s). 22,29,31 However, this pressure was several orders of magnitude higher than the internal pressure of the silkworm. Simulations by Moriya et al. performed under in vivo pressures equivalent to the silkworm blood pressure (0.017 MPa) and atmospheric pressure (0.1 MPa) showed no fiber formation due to the low extrusion pressure.³³ Simulations by Sparkes and Holland that incorporated biological constraints revealed that silk fiber extrusion occurs under extrusion pressures in the range of 6-13 MPa and pultrusion pressure (axial stresses) of 3-12 MPa were generated during forced winding in experiments.³⁴ Moreover, it has been suggested that fibroin fibril formation was triggered by exceeding the criteria of energy accumulation from shear stress, shear rate, or

Evidently, the current understanding of fibroin fiber formation based solely on shear stress is insufficient, and there is a need to explore additional mechanical factors that may contribute to fibrillation. In the spinning duct of a silkworm, there is a silk press, which is a region covered with chitin plates. A 3D structure of the spinning duct shows that the cross-sectional area decreases sharply at the site where the silk press begins. Thus, the chitin plates compress the duct and fibroin may be subjected to significant external forces at this site. Moreover, there is a sharp increase in birefringence due to fibrillation near the boundary between the common duct and the silk press.²² This suggests that the pressure applied to liquid silk in the silk press, in addition to shear stress, may cause fibroin fiber formation. Therefore, this work focuses on pressure as a key parameter for understanding the structural transition from liquid silk (Silk I) to solid silk (Silk II)."

NMR experiments in which pressure is applied by magic angle spinning (MAS) are an excellent means of introducing pressure to liquid samples in a quantitative manner^{37–40} while simultaneously measuring the pressure-induced changes in the structure and dynamics of biomacromolecules. For example, fast MAS NMR has been used to investigate the influence of pressure on retinal chromophore, revealing that a pressureinduced shift in the local dynamics of retinal triggers its isomerization. In addition, the pressure-adapted state of bacteriorhodopsin in the vicinity of retinal was successfully characterized using this technique. 37-39 The structural change of the liquid silk of Samia cynthia ricini was studied using ¹³C MAS NMR, and molecular aggregation was observed.⁴⁰ Other NMR experiments have been performed in which the pressure is applied by a pressure pump. A notable example is an experiment in which hen lysozyme with an amyloid fibril structure, which was initially prepared at 0.1 MPa, was shown to almost fully return to its native state at 0.1 MPa when subjected to a high pressure of 400 MPa.⁴¹

In this study, we investigated the impact of pressure on the structural transition of B. mori liquid silk using ¹³C solid-state MAS NMR. Pressure was applied to the sample by MAS at an appropriate frequency, which enabled us to accurately control

the pressure and detect the structural transition and morphological changes of the liquid silk in real time. We employed a combination of ¹³C cross-polarization (CP)-MAS and direct excited and dipolar decoupled (DD)-MAS NMR measurements to observe the conformation and dynamics of the crystalline region during the transition from the condensed fluid state to the solid state. Upon dehydration of the condensed fluid state of liquid silk, crystalline and amorphous components emerge. The crystalline component in the solid state is called Silk I. In this article, we labeled the molecular structure of liquid silk with a repeated type II β -turn structure in the fluid condensate state precursor Silk I (Silk I_n) (Figure S2a). When the liquid silk is spun into fibroin fibers, the crystalline component of the fiber (that is, Silk II) has a stacked lamellar structure formed by antiparallel β -sheet and β turn structures and was designated herein as Silk II_n (Figure S2b). In this study, we investigated the real-time structural transition from Silk I_p to Silk II_p in the hydrated state under pressure induced by MAS using solid-state NMR experiments. Notably, this is the first time that the pressure-dependent structural transition of liquid silk has been monitored in vitro using NMR. Furthermore, the detailed mechanisms of the pressure-induced conformational transition from Silk I_p to single lamellar Silk II_n and the molecular assembly from Silk I_n to stacked lamellar Silk II_n were detected and analyzed for the first time.

2. MATERIALS AND METHODS

2.1. Sample Preparation. B. mori larvae were received on the first day of the fifth instar (Ehime Sanshu Co., Ehime, Japan). Uniformly ¹³C-labeled liquid silk was biosynthetically prepared by feeding the larvae with 100 mg of U-13C D-glucose (99% enrichment, CIL, USA) and 2 g of an artificial diet (Silk Mate 2M, Nippon Nosan Kogyo Co., Tokyo, Japan) per day from the third to fifth day of their fifth instar. From the sixth day to maturity, only the artificial diet was fed. Silk glands containing liquid silk were extracted from the mature larvae. The posterior part of the middle silk gland was placed in an NMR rotor with a 3.2 mm outer diameter. The inserted sample volume was 30-50 mg. Caps were glued to the sleeve with an epoxy adhesive (Araldite), and NMR measurements were conducted after the adhesive had thoroughly dried.

2.2. Solid-State NMR Measurements. All solid-state NMR experiments were conducted by using a 600 MHz JEOL RESONANCE ECA600-II spectrometer equipped with a 3.2 mm outer diameter double-resonance MAS probe. The 13 C DD-MAS NMR spectra were recorded with a 6.0 μ s 13 C 90° pulse, 57 kHz twopulse phase-modulated (TPPM)⁴² ¹H decoupling during acquisition, and 5 s recycle delay. The ¹³C CP-MAS NMR spectra were recorded with a 3 ms constant CP pulse, 108 kHz TPPM ¹H decoupling, and a 5 s recycle delay. In the DD- and CP-NMR measurements, 1000 transients were accumulated. Consecutive 13C DD- and CP-MAS experiments were performed alternately to monitor the structural transition of the liquid silk. Signals of the mobile groups (Silk I_p) were obtained using the DD-MAS method, and those of the rigid groups (Silk II_p) were obtained by using the CP-MAS method. To examine the effect of pressure variation induced by the MAS frequency on the kinetics of the structural transition, a set of ¹³C DD- and CP-MAS NMR spectra was collected at MAS frequencies of 8, 10, and 15 kHz. The 13 C spin-lattice relaxation times (T_1^{C}) were measured for liquid silk samples that had been subjected to time-course ¹³C MAS NMR for 92.9 h. We used a pulse sequence developed by Torchia et al. 43 for the ${T_1}^{\rm C}$ measurements, which were conducted with a 3 ms ramped CP pulse, 108 kHz TPPM 1 H decoupling, 8 kHz MAS frequency, and 5 s recycle delay. NMR spectra were collected with 1000 scans using an arrayed variable delay of 0.01-2.0 s followed by Fourier transformation. The ¹³C chemical shifts were calibrated externally by using the methylene peak of adamantane at 28.8 ppm, referenced to the

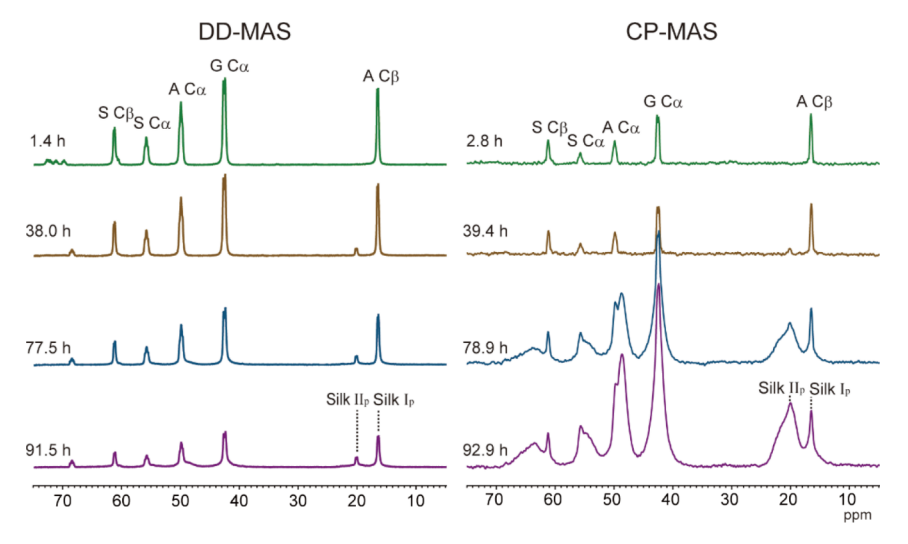


Figure 1. Series of ¹³C DD- and CP-MAS NMR spectra of U-¹³C-labeled B. mori liquid silk conducted alternately at an MAS frequency of 8 kHz (1.32 MPa). Spectra measured 1.4, 38.0, 77.5, and 91.5 h (DD-MAS) and 2.8, 39.4, 78.9, and 92.9 h (CP-MAS) after the start of the series of measurements are shown. A, G, and S denote alanine, glycine, and serine, respectively.

TMS peak at 0 ppm. All spectra were processed using JEOL Delta

2.3. Application of MAS-Induced Hydrostatic Pressure to Liquid Silk. MAS-induced hydrostatic pressure was applied to the liquid silk samples. A liquid silk sample of mass m was packed into a cylindrical MAS rotor with an inner radius of r_0 (Figure S3a). When the liquid silk sample spins with an angular velocity ω , the centrifugal force F at a distance r from the center of the rotor is given by

$$F = mr\omega^2 = 4\pi^2 mr\nu^2 \tag{1}$$

where ν denotes the MAS frequency. When a liquid-state sample is inserted into a cylindrical tube with length l, the volume V of the sample in a cylindrical layer of radius r and layer width dr is given by

$$V = 2\pi l r dr \tag{2}$$

The mass m of the sample can thus be calculated by using its density ρ :

$$m = \rho V = 2\pi l \rho r dr \tag{3}$$

Then, the centrifugal force at a distance r from the center of the cylindrical layer, dF, can be calculated as

$$dF = 8\pi^3 l \rho \nu^2 r^2 dr \tag{4}$$

The total centrifugal force F_0 on the inner walls of the entire sample in the sample tube can be obtained by integrating r from r = 0 (at the center of the tube) to $r = r_0$ (at the inner walls):

$$F_0 = (8\pi^3/3)l\rho v^2 r_0^3 \tag{5}$$

Finally, the pressure P_0 on the inner walls of the sample tube can be obtained by dividing F_0 by the area $A = 2\pi r_0 l$ of the inner sample

$$P_0 = F_0/A = (4\pi^2/3)r_0^2 \nu^2 \rho \tag{6}$$

Various MAS frequencies were used for the pressure variation experiments using an MAS sample tube with an inner diameter of 2.2 mm (Figure S3b). The sample density was found to be 1.30 g/cm³. Thus, using eq 6, the applied pressures at MAS frequencies of 8, 10, and 15 kHz were calculated to be 1.32, 2.07, and 4.65 MPa, respectively. Because the MAS frequency was accurately controlled, the pressure applied by the MAS frequency was stable during the NMR observations.

The pressure P_0 obtained from eq 6 corresponds to the pressure at the inner wall of the cylindrical sample tube. However, when the liquid sample fills the cylindrical tube, the applied pressure at the sample during MAS varies from P_0 (at the inner walls (r_0)) to zero (at

the center of the tube) as a function of the square of the radius, as shown in Figure S3c. Therefore, the pressure values used in this work represent the maximum pressures within the tube (at the inner walls), and the reaction occurs under a pressure gradient as exerted by MAS. Nevertheless, previous studies have shown that protein molecules are typically concentrated near the inner walls during MAS experi-⁴ therefore, these values are expected to accurately represent the MAS-generated pressures on the liquid silk molecules.

3. RESULTS

3.1. Time-Course 13C DD- and CP-MAS Spectra of Liquid Silk under MAS. Alternating sequential ¹³C DD- and CP-MAS measurements were performed for U-13C glucoselabeled liquid silk. A time-dependent structural transition from Silk I_p to Silk II_p was observed under the pressure applied by MAS. Figure 1 shows the ¹³C DD- and CP-MAS spectra obtained at a MAS frequency of 8 kHz together with the assignments of the major peaks; the spectra shown correspond to the first (DD-MAS: 1.4 h, CP-MAS: 2.8 h), 14th (38.0, 39.4 h), 28th (77.5, 78.9 h), and 33rd (91.5, 92.9 h) NMR measurements.

The B. mori fibroin crystalline region mainly consists of repetitive (GAGAGS)_n sequences, with Gly accounting for 46%, Ala for 30%, and Ser for 12% of the total amino acid content. All these peaks were observed in both the CP- and DD-MAS spectra of the same sample, and the assignments of these peaks were accomplished based on previous studies. 15 In the first DD-MAS spectrum, the peaks were assigned to the Gly, Ala, and Ser residues in Silk Ip; the intensities of these peaks decreased over time. In the first CP-MAS spectrum, all of the peaks were derived from Silk Ip, similar to those in the DD-MAS spectrum. However, in the 14th measurements (38.0 and 39.4 h after the start of the DD- and CP-MAS measurements, respectively), a small peak appeared at 20.2 ppm in both the DD- and CP-MAS spectra. This signal is attributed to an intermediate in the pathway from Silk I_p to Silk II_p and corresponds to a β -sheet structure based on the chemical shift values. This intermediate was hypothesized to be a single lamellar Silk II_p, which consists of both β -sheet and β turn structures (Figure S2b). At 78.9 h, strong, broad peaks appeared in the CP-MAS spectrum. These peaks were assigned to the Gly, Ala, and Ser residues of stacked lamellar Silk II,

molecules, which have larger molecular sizes; the intensities of these peaks grew over time, as can be seen from the spectrum measured at 92.9 h.

3.2. Silk II_p **Structure Formed under MAS.** To confirm that the structure that formed under MAS conditions was Silk II_p, we deconvoluted the ¹³C CP-MAS spectrum of Ala $C\beta$ measured at the end of the transformation was deconvoluted. Figure 2 shows the expanded Ala $C\beta$ peak with deconvoluted

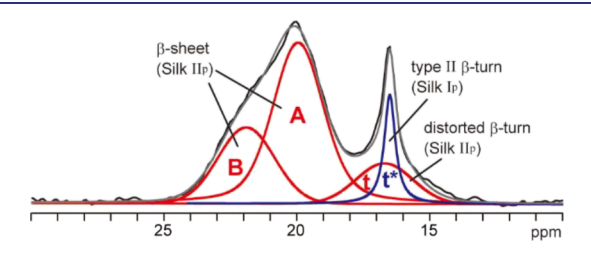


Figure 2. Deconvoluted Ala Cβ peaks from the 13 C CP-MAS spectrum of liquid silk were measured 92.9 h after the start of the measurements at a MAS frequency of 8 kHz (1.32 MPa). It consists of a sharp Silk I_p peak (t*: 16.5 ppm), a broad β-turn peak in Silk II_p (t: 16.7 ppm), and two antiparallel β-sheet peaks in Silk II_p (A: 20.0 ppm, B: 21.9 ppm). Peaks A-t are assigned to the peaks of Ala(A), Ala(B), and Ala(t) in Silk II_p, respectively, as shown in Figure S2. Peak t* is assigned to the type II β-turn in Silk I_p.

peaks of the ^{13}C CP-MAS spectrum measured 92.9 h after the start of the measurement at a MAS frequency of 8 kHz (1.32 MPa). The deconvolution showed that the Ala C β peak was composed of four components: two β -sheet components derived from stacked lamellar Silk II $_{\rm p}$ (Ala(A): 20.0 ppm; Ala(B): 21.9 ppm), a distorted β -turn component derived from stacked lamellar Silk II $_{\rm p}$ (Ala(t): 16.7 ppm), and a sharp β -turn component derived from Silk I $_{\rm p}$ (Ala(t*): 16.5 ppm).

After applying pressure to the liquid silk by MAS, the percentages of the Ala(A), Ala(B), Ala(t), and Ala(t*) components were determined to be 52, 26, 14, and 8%, respectively (Table 1). The chymotrypsin treatment of fibroin

Table 1. Chemical Shifts of Ala C β in the CP-MAS NMR Spectrum at 92.9 h^a

type of $C\beta$	chemical shift (ppm)	fraction (%)	Cp fraction (%) ¹⁶	secondary structure
Ala(t*) (silk I _p)	16.5	8		type II β -turn
Ala(t) (silk II _p)	16.7	14	32	distorted β -turn
Ala(A) (silk II _p)	20.0	52	45	β -sheet
Ala(B) (silk II _p)	21.7	26	23	eta-sheet

^aThe positions of Ala(t), Ala(A), and Ala(B) in the lamellar structure are shown in Figure S2b.

fibers yields fibroin with only a crystalline component (Cp fraction), that is, only fibroin-forming Silk II. ⁴⁵ In the deconvoluted Ala C β spectrum, the Cp fraction of Ala(A) (peak A at 20.0 ppm), situated at the center of the β -sheets in the lamellar structure (see Figure S2b), was 45%; that of Ala(B) (peak B at 21.9 ppm), which corresponds to the β -sheet regions next to the turns in the lamellar structure, was 23%; and that of Ala(t) (peak t at 16.7 ppm), which corresponds to the distorted β -turns of stacked lamellar Silk II_p (Figure S2b), was 32%. ¹⁶ Therefore, the β -sheet(A)-to- β -

sheet(B) ratio of the Cp fraction was approximately 2:1. The β -sheet(A)-to- β -sheet(B) ratio of the structure formed under MAS conditions was also approximately 2:1. The lower fraction of the distorted β -turn(t) component is likely due to differences in hydration rates between fibroin in the NMR sample and fibroin fibers. Thus, the higher mobility of the distorted β -turn component compared to that of the β -sheet region may have reduced its CP efficiency, resulting in a relatively lower fraction of the distorted β -turn component. These results clearly show that the product of the MAS experiments was stacked lamellar Silk II $_{\rm p}$, which had the same Cp fraction as the generated fibroin fiber.

3.3. Time Dependence of Peak Intensity for Silk I_p and Silk II_p under MAS. Figure 3 shows plots of the Ala $C\beta$

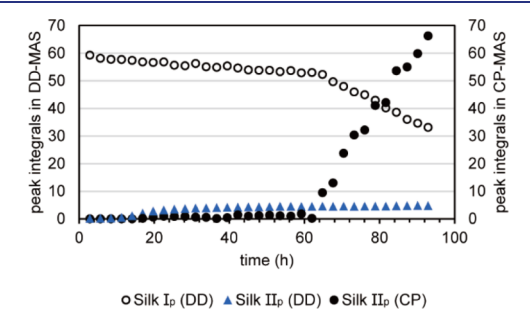


Figure 3. Time dependence of Ala $C\beta$ peak integrals of liquid silk for Silk I_p peak (\bigcirc) observed in the 13 C DD-MAS NMR spectra, Silk II_p peak (\bigcirc) observed in the 13 C CP-MAS NMR spectra, and Silk II_p peak (\bigcirc in blue) observed in the 13 C DD-MAS NMR spectra with a MAS frequency of 8 kHz (1.32 MPa).

peak intensities for the Silk I_p (\bigcirc) and single lamellar Silk II_p (A) components in the DD-MAS spectra and the stacked lamellar Silk II_p (\bullet) component in the CP-MAS spectra versus time at a MAS frequency of 8 kHz (1.32 MPa). In the CP-MAS spectra, a stacked lamellar Silk II_p peak (●) appeared after 60 h and then rapidly increased in intensity between 60 and 92.9 h. Correspondingly, in the DD-MAS spectrum, the intensity of the Silk Ip peak slightly decreased from the start of the measurement to 60 h and then decreased rapidly from 60 to 92.9 h. This decrease in the intensity of the Silk I_p peak after 60 h is consistent with the growth of stacked lamellar Silk II_p, as inferred from the CP-MAS spectra. Similar changes were observed for the Gly C α , Ala C α , Ser C α , and Ser C β peaks in the CP- and DD-MAS spectra, as shown in Figure S4. This result demonstrates that the crystalline region consisting of (GAGAGS), sequences underwent a structural transition from Silk $I_{\scriptscriptstyle D}$ to stacked lamellar Silk $II_{\scriptscriptstyle D}$ structures.

In addition to the Silk I_p peak, a small peak corresponding to single lamellar Silk II_p was observed at 20.2 ppm in the DD-MAS spectrum (Figure 1; 38.0 h). This peak appeared after approximately 14 h and slightly increased in intensity until approximately 40 h, as shown by the blue triangles in Figure 3. However, its intensity was lower than that of the Silk I_p peak and remained constant until the end of the measurement. Therefore, based on the DD-MAS spectra, Silk II_p is expected to have a mobile single lamellar β -sheet structure. Based on the change of the Silk II_p peak integral in the DD-MAS spectra, the following model can be proposed for the structural transition of Silk I_p to Silk II_p : Silk I_p molecules transform into single lamellar β -sheet structures, which produce a Silk II_p peak in the DD-MAS spectra. These structures act as intermediates that

react with Silk $\rm I_p$ to form Silk $\rm II_p$ with stacked lamellar β -sheet structures, as indicated by the Silk $\rm II_p$ peak in the CP-MAS spectrum.

3.4. T_1^{C} Measurements of Liquid Silk after the Pressurization. The signal intensity decay due to T_1^{C} relaxation was measured after the structural transition by applying pressure to the sample via MAS (Figure 4). The T_1^{C}

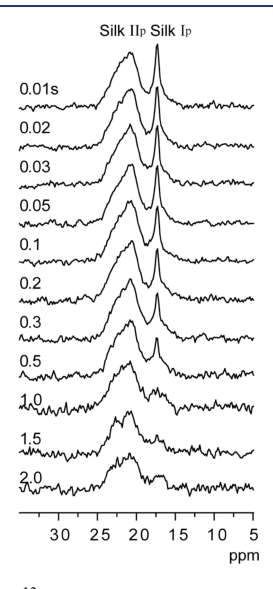


Figure 4. Spectra of $^{13}\mathrm{C}$ spin—lattice relaxation time in an Ala $C\beta$ region with a variable delay of 0.01 to 2.0 s. Both Silk $\mathrm{I_p}$ and Silk $\mathrm{II_p}$ peaks were observed because the measurements were conducted using a CP pulse after alternating $^{13}\mathrm{C}$ CP- and DD-MAS measurements.

values for both the Silk $\rm I_p$ and Silk $\rm II_p$ Ala and Ser peaks are listed in Table 2. For all of the peaks, the $T_1^{\rm C}$ values for Silk $\rm II_p$

Table 2. 13 C Spin-Lattice Relaxation Times of Ala and Ser Residues in Silk I_p and Silk II_p Molecules

	silk I _p	silk II _p
	$T_1^{C}(s)$	$T_1^{C}(s)$
Ala C α	0.98 ± 0.058	2.56 ± 0.045
Ala C β	0.52 ± 0.013	1.50 ± 0.032
Ser C α	0.98 ± 0.034	3.09 ± 0.015
Ser Cβ	0.29 ± 0.029	3.64 ± 0.019

were longer than those for Silk Ip, indicating that Silk IIp was less mobile than Silk I_p . Silk II_p consists of a β -sheet structure with hydrogen bonds between the intermolecular main-chain amide and OH groups; as the formation of the stacked β -sheet structure enlarges the molecular size of Silk II_p, it is less mobile than Silk I_p . Furthermore, Ser $C\beta$ had both the lowest T_1^C value in Silk I_p and the highest T_1^C value in Silk II_p , implying that Ser $C\beta$ has the highest mobility in Silk I_p , and conversely the lowest mobility in Silk II_p. This is attributed to the OH groups of the Ser side chains, which interact with the water molecules in Silk Ip. Moreover, the OH groups form intra- and intermolecular hydrogen bonds through water molecules, which limits the dynamics of Ser C β in Silk II_p. In the dry state, parts of Ser C β in Silk II_p form hydrogen bonds with intra- and/or inter- β -strands, while other parts of Ser C β do not form hydrogen bonds, indicating that there are two components each with separate T_1^{C} values for Ser C β . It was also noted that the T_1^{C} values of Ala C α and Ser C α were

almost the same, indicating that the motion of the backbone in the β -sheets was similar at both the Ala C α and Ser C α positions.

3.5. Influence of MAS Frequency on Structural Transition. The growth behaviors of the normalized Ala $C\beta$ peak intensities of Silk II_p in the ¹³C CP-MAS spectra at 8, 10, and 15 kHz were plotted against elapsed time (Figure 5). The

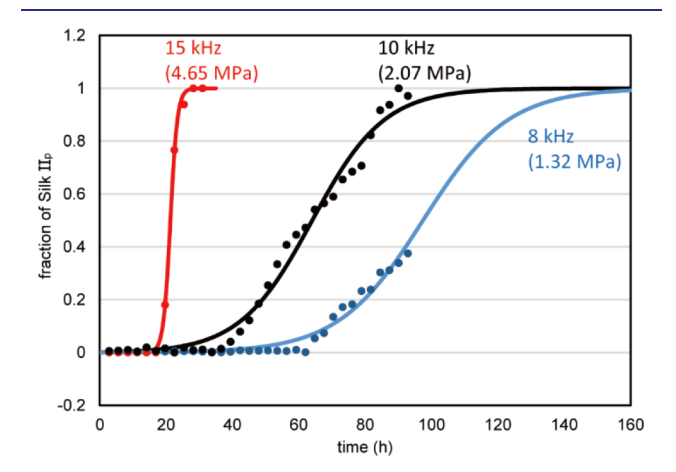


Figure 5. Time dependence of normalized Silk II_p peak integrals observed in the 13 C CP-MAS NMR spectra for Ala C β at various MAS frequencies (8, 10, and 15 kHz). The data were fit to a two-step kinetic model (solid lines).

fractions of Silk II_p at 8 kHz were extrapolated based on the final fraction of 0.375 obtained from the decay of the DD-MAS signal. The higher the MAS frequency, the greater the pressure applied to the sample. The pressure was calculated using eq 6 to be 1.32, 2.07, and 4.65 MPa at 8, 10, and 15 kHz, respectively. Notably, the growth rate of stacked lamellar Silk II_n increased at higher pressures. Although the mechanism of the two-step process from nucleation to structural transition is suggested to be the same at 8, 10, and 15 kHz, the speed of the transition varied significantly. The lag times for the structural transition from Silk I_p to Silk II_p were 62, 36, and 17 h at 8, 10, and 15 kHz, respectively. Importantly, the structural transition accelerated significantly with increasing MAS frequency, corresponding to an increasing pressure. Clearly, the greater the pressure applied to the liquid silk, the shorter the lag time required for nucleation and the faster the structural transition progresses.

4. DISCUSSION

4.1. Pressure Generation in Protein Solution by MAS.

It has been reported that MAS leads to protein sedimentation on the inner wall of the MAS rotor. Consequently, researchers have raised concerns that variations in the MAS frequency could introduce differences not only in pressure but also in the protein concentration gradient. Therefore, to understand the effect of pressure on the protein solution during the MAS experiments, we examined the relationship between the fibroin concentration and distance from the rotating axis in our experiments using previously published formulas. As shown in Figure S5, fibroin molecules are proposed to concentrate on the inner wall of the MAS sample tube with a width of 0.15 mm and protein concentration of $4.0C_0$, where C_0 is the initial concentration of fibroin without spinning. The relationship between the distance from the

rotating axis and the fibroin concentration is calculated to be almost the same at 8, 10, and 15 kHz, corresponding to pressures of 1.32, 2.07, and 4.65 MPa, respectively. From this, it was concluded that the main factor affecting fibroin at different MAS frequencies was the static pressure at the inner wall of the MAS rotor. It should be mentioned that condensed fibroin molecules remain in the fluid state under MAS conditions because the DD-MAS signals of Silk I_p were much stronger than the CP-MAS signals during the initial stages of sample spinning.

4.2. Kinetic Analysis for the Mechanism of the Transition from Silk I_p to Silk II_p under Pressure. In this section, detailed kinetic analyses of the transition from Silk I_p to Silk II_p under pressure are discussed. Figure 5 shows the rate of the transition from Silk I_p to Silk II_p under different pressures. At each pressure, there was a lag before the transition began. After the lag period, the transition from Silk I_p to Silk II_p accelerated. As the CP-MAS signal intensity increased, the oligomerization of Silk IIp, which enlarges the stacked lamellar structure, occurred simultaneously with the transition of Silk I_p to Silk II_p, as shown schematically in Figure 6. This kinetic behavior is similar to that of amyloid fibril

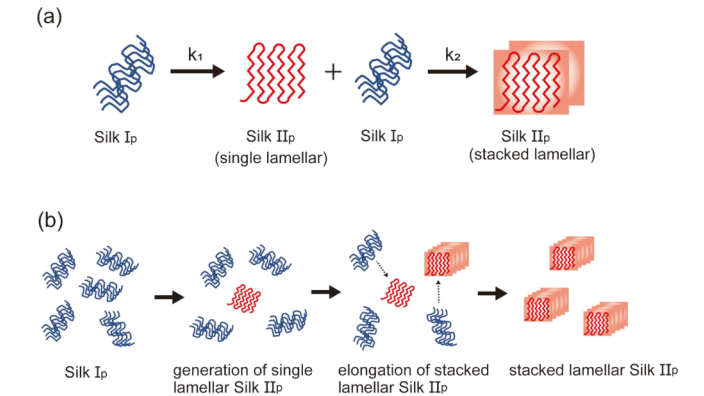


Figure 6. Schematic of proposed models for the pressure-induced structural transition from Silk I_p to stacked lamellar Silk II_p. (a) Twostep transformation of Silk I_p to stacked lamellar Silk II_p ; k_1 and k_2 represent the rate constants of the first and second reactions, respectively. (b) Time course of the pressure-induced structural transition of Silk I_p to Silk II_p via a two-step autocatalytic reaction.

formation in human calcitonin (hCT):46,47 hCT monomers (α -helix) first form an oligomeric fibril intermediate (β -sheet), which then reacts with hCT monomers to elongate the hCT fibrils by acting as a catalyst in the second step. This is known as a two-step autocatalytic reaction.

In the case of silk fibroin, the mechanism behind the formation of stacked Silk II_p from Silk I_p was assumed to be a similar two-step autocatalytic reaction. In the liquid silk fibroin system, liquid silk initially forms a Silk I_p structure (Figure S2a), which is a repeated type II β -turn structure. ⁷⁻⁹ Silk I_n molecules are very mobile, as observed in the DD-MAS experiments, with short relaxation times, as shown in Table 2. In the first step, the Silk I_p molecules change into Silk II_p, hypothesized to have a single lamellar structure, which is an intermediate in the first step of the reaction (Figure 6a). This reaction is expressed as a nucleation step with the rate constant k_1 :

Silk
$$I_p \rightarrow Silk II_p$$
(single lamellar state) (7)

This can be expressed using the following differential equation:

$$\left(\frac{\mathrm{d}f}{\mathrm{d}t}\right)_{1} = k_{1}(1-f) \tag{8}$$

where f is the fraction of Silk II_D molecules and k_1 is the rate constant of the first reaction step. In the second step, Silk II_p (n stacked lamellar) molecules react with Silk I_p molecules, and Silk I_p changes to Silk II_p (n + 1 stacked lamellar):

Silk $II_p(n \text{ stacked lamellar}) + Silk I_p$

$$\rightarrow$$
 Silk II_p($n + 1$ stacked lamellar) (9)

This can be expressed using the following differential

$$\left(\frac{\mathrm{d}f}{\mathrm{d}t}\right)_2 = k_2 a f(1-f) \tag{10}$$

where k_2 is the rate constant of the second reaction step and ais the initial concentration of Silk I_p molecules. This occurs because the polypeptide unit $(GAGAGS)_n$ (n > 3) can form a Silk I_p (repeated β -turn structure) unit and transforms into a single lamellar structure, 16,17 as shown in Figure 6a. We considered the unit number of the lamellar-forming sequence, $(GAGAGS)_n$ (n > 3), as the concentration of Silk I_p molecules that changed to Silk II_p (lamellar) molecules. In this reaction, Silk II_p molecules act as catalysts to convert Silk I_p into Silk II_p. Therefore, the reaction from Silk I_p to stacked Silk II_p is proposed to be a two-step autocatalytic reaction, similar to that of hCT amyloid fibril formation.

We analyzed the rate constants k_1 and k_2 using the following equation after integrating the sum of the differential equations of the first and second reaction steps: 46,47

$$f = \frac{\sigma\{\exp[(1+\sigma)kt] - 1\}}{\{1 + \sigma\exp[(1+\sigma)kt]\}}$$
(11)

where f is the fraction of Silk II_p molecules in the fibril form at time t, σ represents a dimensionless description of rates k_1 to k_2 $(\sigma = k_1/k \text{ and } k = ak_2)$, and a is the initial concentration of Silk I_p units. In the estimation of the initial concentration, we took the number of $(GAGAGS)_n$ (n > 3) units, which are the 48 units existing in the H chain of silk fibroin molecules (7.8 × 10⁻⁴ M). Furthermore, it is anticipated that the fibroin molecules become four times more concentrated on the inner wall by MAS. Then, the initial unit concentration a was estimated to be 0.15 M.

The best-fit curves were evaluated using eq 11, as indicated by the solid lines in Figure 5, and the rate constants $(k_1 \text{ and } k_2)$ were calculated and are summarized in Table 3. The k_1 values were very small, and those at the highest pressure (4.65 MPa) were much smaller than those under pressures of 2.07 and 1.32 MPa. In contrast, the k_2 value was significantly higher at 4.65 MPa than those at 2.07 and 1.32 MPa. The large difference

Table 3. Reaction Rate Constants k_1 and k_2 from the Kinetics Curves for the Structural Transition from Silk I_p to Silk II_p under Various MAS Frequencies

MAS frequency (kHz)	pressure (MPa)	$k_1 \; ({ m s}^{-1})$	$k_2 \; (\mathrm{M}^{-1} \; \mathrm{s}^{-1})$
8	1.32	$1.10 \ (\pm \ 2.16) \times 10^{-8}$	$1.44 (\pm 0.09) \times 10^{-4}$
10	2.07	$7.16 (\pm 0.23) \times 10^{-8}$	$1.70 \ (\pm \ 0.09) \times 10^{-4}$
15	4.65	$8.68 (\pm 0.40) \times 10^{-13}$	$1.70 \ (\pm \ 0.08) \times 10^{-3}$

between k_1 and k_2 caused a lag time for the transition from Silk I_p to Silk II_p; however, the production of Silk II_p fibrils increased sharply after the lag time, and the lag time became shorter at larger k_2 values.

The kinetic analysis of the transition from Silk I_p to Silk II_p under pressure revealed the following points. (1) The transition from Silk I_p to Silk II_p can be considered to be a two-step autocatalytic reaction. (2) In the first step, Silk I_p transforms into single lamellar Silk IIp, which acts as an intermediate. (3) In the second step, single lamellar Silk II_p reacts with Silk I_p units to form larger stacked lamellar Silk II_p regions, where the single lamellar Silk II_p units act as catalysts. This second-step reaction indicates that the pressure-induced structural change affects not only the secondary structure but also the stacking size of stacked lamellar Silk II_p, resulting in the production of a robust silk fiber. (4) The rate constant k_2 in the second step is strongly dependent on the pressure: a higher pressure results in a much larger k_2 value. (5) However, the k_1 values are much smaller than the k_2 values, which causes a long lag time for the growth of stacked lamellar Silk II_p. (6) Notably, at 4.65 MPa—the pressure most similar to the actual extrusion pressure applied at the spinneret in silkworms—the lag time is the shortest and the growing speed the highest, despite the k_1 value being the lowest at this pressure. The result that the k_1 value at 4.65 MPa is several orders of magnitude smaller than those at 2.07 and 1.32 MPa seems excessively small. This can be justified by improving the precision of the experiment, such as conducting more accurate measurements of the sample concentration or by considering a revision of the fitting model.

It is of interest to discuss how Silk I_D molecules transition to Silk II_p fibrils in the spinneret to form silk fibers. Fibril formation has been shown to occur in the spinneret at pressures of 1–50 MPa,²⁸ a range that was later refined to 6– 13 MPa under more natural conditions.³⁴ Briefly, our results indicate that silk fibroin undergoes a structural change from Silk I_p to Silk II_p in this pressure range (Figure S1).

We observed that pressurization accelerates the reaction rate of the second step of the autocatalytic stacking reaction in the structural transformation from Silk I_p to Silk II_p, although there is a long lag time before the onset of the formation of stacked lamellar Silk II_p. Based on these results, the natural spinning process of silkworms is proposed as follows. When new liquid silk is transported to the silk press, some of the Silk II, molecules that were formed previously in the spinneret will also be present. It is postulated that after the liquid silk is transported to the silk press in the spinneret and pressurized via the extrusion process, stacked lamellar Silk II_p can be produced very quickly without lag time. This process has been reported as seeding effects in the amyloid fibril formation.⁴⁸ This hypothesis explains how silkworms quickly produce Silk II_p fibrils at the spinneret during the spinning process.

5. CONCLUSIONS

The mechanism of the structural transition of B. mori liquid silk fibroin was investigated using solid-state NMR under pressure applied by MAS. The transition from Silk I_p to Silk II_p was observed in liquid silk by detecting the changes in the positions of the Ala C β signals in the CP-MAS spectra. The formation of stacked lamellar Silk II_p begins after a certain lag time and consequently accelerates to form the larger stacked lamellar Silk II_p. This kinetic profile proposes that the transition from Silk I_p to Silk II_p occurs via a two-step

autocatalytic reaction in which repeated β -turn Silk I_p changes to single lamellar Silk II_p as an intermediate in the first step, after which single lamellar Silk II_p reacts with Silk I_p to form stacked lamellar Silk II_p in the second step. The single lamellar Silk II_p units, therefore, act as catalysts to accelerate the formation of the larger stacked lamellar Silk II_p. In addition, we found that the rate of the second step became faster under higher pressures. Based on these results, we proposed that the transition from liquid silk (Silk I) to silk fibers (Silk II) occurs rapidly after a very short lag time in the spinneret of silkworms by applying a pressure of approximately 5 MPa in the presence of lamellar Silk II_p units, which serve as seeds. We believe that these findings will aid in the development and production of robust silk-like fibers.

ASSOCIATED CONTENT

Supporting Information

The Supporting Information is available free of charge at https://pubs.acs.org/doi/10.1021/jacs.3c04361.

Additional figures showing the morphology of the silk gland and the birefringence of liquid silk, structure of Silk I_p and Silk II_p, plot of pressure inside the rotor under MAS, plot of Silk II_p fraction against time, plot of fibroin concentration against the distance from the rotor axis (PDF)

AUTHOR INFORMATION

Corresponding Authors

Yu Suzuki - Department of Applied Chemistry and Biotechnology, Graduate School of Engineering, University of Fukui, Fukui 9108507, Japan; oorcid.org/0000-0002-8043-8015; Email: suzukiyu@u-fukui.ac.jp

Akira Naito - Department of Biotechnology, Tokyo University of Agriculture and Technology, Tokyo 184-8588, Japan; Graduate School of Engineering, Yokohama National University, Yokohama 240-8501, Japan; orcid.org/0000-0003-2443-6135; Email: naito@ynu.ac.jp

Authors

Shota Morie - Department of Applied Chemistry and Biotechnology, Graduate School of Engineering, University of Fukui, Fukui 9108507, Japan

Hideyasu Okamura - Department of Applied Chemistry and Biotechnology, Graduate School of Engineering, University of Fukui, Fukui 9108507, Japan

Tetsuo Asakura – Department of Biotechnology, Tokyo University of Agriculture and Technology, Tokyo 184-8588, Japan; orcid.org/0000-0003-4472-6105

Complete contact information is available at: https://pubs.acs.org/10.1021/jacs.3c04361

The authors declare no competing financial interest.

ACKNOWLEDGMENTS

Y.S. acknowledges support from a Grant-in-Aid for Scientific Research (C) (18K05232).

REFERENCES

(1) Koeppel, A.; Holland, C. Progress and Trends in Artificial Review Silk Spinning: A Systematic Review. ACS Biomater. Sci. Eng. **2017**, 3 (3), 226–237.

- (2) Andersson, M.; Johansson, J.; Rising, A. Silk Spinning in Silkworms and Spiders. *Int. J. Mol. Sci.* **2016**, *17* (8), 1290.
- (3) Qiu, W.; Patil, A.; Hu, F.; Liu, X. Y. Hierarchical Structure of Silk Materials Versus Mechanical Performance and Mesoscopic Engineering Principles. *Small* **2019**, *15* (51), No. 1903948.
- (4) Zhou, C.-Z.; Confalonieri, F.; Jacquet, M.; Perasso, R.; Li, Z.-G.; Janin, J. Silk Fibroin: Structural Implications of a Remarkable Amino Acid Sequence. *Proteins: Struct. Funct. Genet.* **2001**, 44 (2), 119–122.
- (5) Inoue, S.; Tanaka, K.; Arisaka, F.; Kimura, S.; Ohtomo, K.; Mizuno, S. Silk Fibroin of *Bombyx mori* is Secreted, Assembling a High Molecular Mass Elementary Unit Consisting of H-chain, L-chain, and P25, with a 6:6:1 Molar Ratio. *J. Biol. Chem.* **2000**, 275 (51), 40517–40528.
- (6) Zhou, C.-Z.; Confalonieri, F.; Medina, N.; Zivanovic, Y.; Esnault, C.; Yang, T.; Jacquet, M.; Janin, J.; Duguet, M.; Perasso, R.; Li, Z.-G. Fine Organization of *Bombyx mori* Fibroin Heavy Chain Gene. *Nucleic Acids Res.* **2000**, *28* (12), 2413–2419.
- (7) Asakura, T.; Ohgo, K.; Komatsu, K.; Kanenari, M.; Okuyama, K. Refinement of Repeated β -turn Structure for Silk I Conformation of *Bombyx mori* Silk Fibroin Using ¹³C Solid-State NMR and X-ray Diffraction Methods. *Macromolecules* **2005**, 38 (17), 7397–7403.
- (8) Asakura, T.; Ashida, J.; Yamane, T.; Kameda, T.; Nakazawa, Y.; Ohgo, K.; Komatsu, K. A Repeated β -turn Structure in Poly(Ala-Gly) as a Model for Silk I of *Bombyx mori* Silk Fibroin Studied with Two-Dimensional Spin-Diffusion NMR Under Off Magic Angle Spinning and Rotational Echo Double Resonance. *J. Mol. Biol.* **2001**, 306 (2), 291–305.
- (9) Asakura, T.; Naito, A. Structure of Silk I (*Bombyx mori* Silk Fibroin before Spinning) in the Dry and Hydrated States Studied Using ¹³C Solid-State NMR Spectroscopy. *Int. J. Biol. Macromol.* **2022**, 216, 282–290.
- (10) Asakura, T. Structure of Silk I (Bombyx mori Silk Fibroin before Spinning) -Type II β -Turn, Not α -Helix-. Molecules **2021**, 26 (12), 3706.
- (11) Asakura, T.; Sato, H.; Moro, F.; Nakazawa, Y.; Aoki, A. Lamellar Structure in Poly(Ala-Gly) Determined by Solid-State NMR and Statistical Mechanical Calculations. *J. Am. Chem. Soc.* **2007**, *129* (17), 5703–5709.
- (12) Suzuki, Y.; Yamazaki, T.; Aoki, A.; Shindo, H.; Asakura, T. NMR Study of the Structures of Repeated Sequences, GAGXGA (X = S, Y, V), in *Bombyx mori* Liquid Silk. *Biomacromolecules* **2014**, *15* (1), 104–112.
- (13) Marsh, R. E.; Corey, R. B.; Pauling, L. An Investigation of the Structure of Silk Fibroin. *Biochim. Biophys. Acta* **1955**, *16* (1), 1–34.
- (14) Takahashi, Y.; Gehoh, M.; Yuzuriha, K. Structure Refinement and Diffuse Streak Scattering of Silk (*Bombyx mori*). *Int. J. Biol. Macromol.* **1999**, 24 (2–3), 127–138.
- (15) Suzuki, Y.; Aoki, A.; Nakazawa, Y.; Knight, D. P.; Asakura, T. Structural Analysis of the Synthetic Peptide (Ala-Gly-Ser-Gly-Ala-Gly)₅, a Model for the Crystalline Domain of *Bombyx mori* Silk Fibroin, Studied with ¹³C CP/MAS NMR, REDOR, and Statistical Mechanical Calculations. *Macromolecules* **2010**, *43* (22), 9434–9440.
- (16) Asakura, T.; Aoki, A.; Komatsu, K.; Ito, C.; Suzuki, I.; Naito, A.; Kaji, H. Lamellar Structure in Alanine—Glycine Copolypeptides Studied by Solid-State NMR Spectroscopy: A Model for the Crystalline Domain of *Bombyx mori* Silk Fibroin in Silk II Form. *Biomacromolecules* **2020**, *21* (8), 3102—3111.
- (17) Asakura, T.; Ogawa, T.; Naito, A.; Williamson, M. P. Chain-Folded Lamellar Structure and Dynamics of the Crystalline Fraction of *Bombyx mori* Silk Fibroin and of (Ala-Gly-Ser-Gly-Ala-Gly)_n Model Peptides. *Int. J. Biol. Macromol.* **2020**, *164*, 3974–3983.
- (18) Asakura, T.; Umemura, K.; Nakazawa, Y.; Hirose, H.; Higham, J.; Knight, D. Some Observations on the Structure and Function of the Spinning Apparatus in the Silkworm *Bombyx mori. Biomacromolecules* **2007**, 8 (1), 175–181.
- (19) Domigan, L. J.; Andersson, M.; Alberti, K. A.; Chesler, M.; Xu, Q.; Johansson, J.; Rising, A.; Kaplan, D. L. Carbonic Anhydrase Generates a pH Gradient in *Bombyx mori* Silk Glands. *Insect Biochem. Mol. Biol.* **2015**, *65*, 100–106.

- (20) Zhou, L.; Chen, X.; Shao, Z.; Huang, Y.; Knight, D. P. Effect of Metallic Ions on Silk Formation in the Mulberry Silkworm *Bombyx mori. J. Phys. Chem. B* **2005**, *109* (35), 16937–16945.
- (21) Holland, C.; Urbach, J. S.; Blair, D. L. Direct Visualization of Shear Dependent Silk Fibrillogenesis. *Soft Matter* **2012**, *8* (9), 2590–2594.
- (22) Moriya, M.; Roschzttardtz, F.; Nakahara, Y.; Saito, H.; Masubuchi, Y.; Asakura, T. Rheological Properties of Native Silk Fibroins from Domestic and Wild Silkworms, and Flow Analysis in Each Spinneret by a Finite Element Method. *Biomacromolecules* **2009**, *10* (4), 929–935.
- (23) Boulet-Audet, M.; Terry, A. E.; Vollrath, F.; Holland, C. Silk Protein Aggregation Kinetics Revealed by Rheo-IR. *Acta Biomater.* **2014**, *10* (2), 776–784.
- (24) Terry, A. E.; Knight, D. P.; Porter, D.; Vollrath, F. pH Induced Changes in the Rheology of Silk Fibroin Solution from the Middle Division of *Bombyx mori* Silkworm. *Biomacromolecules* **2004**, *5* (3), 768–772.
- (25) Ochi, A.; Hossain, K. S.; Magoshi, J.; Nemoto, N. Rheology and Dynamic Light Scattering of Silk Fibroin Solution Extracted from the Middle Division of *Bombyx mori* Silkworm. *Biomacromolecules* **2002**, 3 (6), 1187–1196.
- (26) Jin, Y.; Hang, Y.; Luo, J.; Zhang, Y.; Shao, H.; Hu, X. *In Vitro* Studies on the Structure and Properties of Silk Fibroin Aqueous Solutions in Silkworm. *Int. J. Biol. Macromol.* **2013**, *62*, 162–166.
- (27) Laity, P. R.; Holland, C. The Rheology behind Stress-Induced Solidification in Native Silk Feedstocks. *Int. J. Mol. Sci.* **2016**, *17* (11), 1812.
- (28) Ohgo, K.; Bagusat, F.; Asakura, T.; Scheler, U. Investigation of Structural Transition of Regenerated Silk Fibroin Aqueous Solution by Rheo-NMR Spectroscopy. *J. Am. Chem. Soc.* **2008**, *130* (12), 4182–4186.
- (29) Breslauer, D. N.; Lee, L. P.; Muller, S. J. Simulation of Flow in the Silk Gland. *Biomacromolecules* **2009**, *10* (1), 49–57.
- (30) Bratzel, G.; Buehler, M. J. Molecular Mechanics of Silk Nanostructures Under Varied Mechanical Loading. *Biopolymers* **2012**, 97 (6), 408–417.
- (31) Kojic, N.; Kojic, M.; Gudlavalleti, S.; McKinley, G. Solvent Removal during Synthetic and *Nephila* Fiber Spinning. *Biomacromolecules* **2004**, *5* (5), 1698–1707.
- (32) Moriya, M.; Ohgo, K.; Masubuchi, Y.; Knight, D. P.; Asakura, T. Micro-Computerized Tomographic Observation of the Spinning Apparatus in *Bombyx mori* Silkworms. *Polymer* **2008**, 49 (26), 5665–5669.
- (33) Moriya, M.; Ohgo, K.; Masubuchi, Y.; Asakura, T. Flow Analysis of Aqueous Solution of Silk Fibroin in the Spinneret of *Bombyx mori* Silkworm by Combination of Viscosity Measurement and Finite Element Method Calculation. *Polymer* **2008**, 49 (4), 952–956.
- (34) Sparkes, J.; Holland, C. Analysis of the Pressure Requirements for Silk Spinning Reveals a Pultrusion Dominated Process. *Nat. Commun.* **2017**, *8* (1), 594.
- (35) Sparkes, J.; Holland, C. The Energy Requirements for Flow-Induced Solidification of Silk. *Macromol. Biosci.* **2019**, *19* (3), No. 1800229.
- (36) Schaefer, C.; Mcleish, T. Theoretical Rheo-Physics of Silk: Intermolecular Associations Reduce the Critical Specific Work for Flow-Induced Crystallization. *J. Rheol.* **2022**, *66*, 515–534.
- (37) Kawamura, I.; Yamaguchi, S.; Nishikawa, H.; Tajima, K.; Horigome, M.; Tuzi, S.; Saito, H.; Naito, A. Change in Local Dynamics of Bacteriorhodopsin with Retinal Isomerization Under Pressure as Studied by Fast Magic Angle Spinning NMR. *Polym. J.* **2012**, *44* (8), 863–867.
- (38) Kawamura, I.; Kihara, N.; Ohmine, M.; Nishimura, K.; Tuzi, S.; Saitô, H.; Naito, A. Solid-State NMR Studies of Two Backbone Conformations at Tyr185 as a Function of Retinal Configurations in the Dark, Light, and Pressure Adapted Bacteriorhodopsins. *J. Am. Chem. Soc.* **2007**, *129* (5), 1016–1017.

- (39) Kawamura, I.; Degawa, Y.; Yamaguchi, S.; Nishimura, K.; Tuzi, S.; Saitô, H.; Naito, A. Pressure-Induced Isomerization of Retinal on Bacteriorhodopsin as Disclosed by Fast Magic Angle Spinning NMR. *Photochem. Photobiol.* **2007**, 83 (2), 346–350.
- (40) Nakazawa, Y.; Nakai, T.; Kameda, T.; Asakura, T. A ¹³C NMR Study on the Structural Change of Silk Fibroin from *Samia cynthia ricini*. Chem. Phys. Lett. **1999**, 311 (5), 362–366.
- (41) Akasaka, K.; Maeno, A. Proteins in Wonderland: The Magical World of Pressure. *Biology* **2022**, *11* (1), 6.
- (42) Bennett, A. E.; Rienstra, C. M.; Auger, M.; Lakshmi, K. V.; Griffin, R. G. Heteronuclear Decoupling in Rotating Solids. *J. Chem. Phys.* **1995**, *103* (16), 6951–6958.
- (43) Torchia, D. A. The Measurement of Proton-Enhanced Carbon-13 T_1 Values by a Method Which Suppresses Artifacts. *J. Magn. Reson.* **1978**, 30 (3), 613–616.
- (44) Bertini, I.; Luchinat, C.; Parigi, G.; Ravera, E.; Reif, B.; Turano, P. Solid-State NMR of Proteins Sedimented by Ultracentrifugation. *Proc. Natl. Acad. Sci. U. S. A.* **2011**, *108* (26), 10390–10399.
- (45) Strydom, D. J.; Haylett, T.; Stead, R. H. The Amino-Terminal Sequence of Silk Fibroin Peptide CP A Reinvestigation. *Biochem. Biophys. Res. Commun.* 1977, 79 (3), 932–938.
- (46) Itoh-Watanabe, H.; Kamihira-Ishijima, M.; Kawamura, I.; Kondoh, M.; Nakakoshi, M.; Sato, M.; Naito, A. Characterization of the Spherical Intermediates and Fibril Formation of hCT in HEPES Solution Using Solid-State ¹³C-NMR and Transmission Electron Microscopy. *Phys. Chem. Chem. Phys.* **2013**, *15* (39), 16956–16964.
- (47) Kamihira, M.; Naito, A.; Tuzi, S.; Saitô, H.; Nosaka, A. Y. Conformational Transitions and Fibrillation Mechanism of Human Calcitonin as Studied by High-Resolution Solid-State ¹³C NMR. *Protein Sci.* **2000**, 9 (5), 867–877.
- (48) O'Nuallain, B.; Williams, A. D.; Westermark, P.; Wetzel, R. Seeding Specificity in Amyloid Growth Induced by Heterologous Fibrils. J. Biol. Chem. 2004, 279 (17), 17490–17499.